Hindawi
Structural Control and Health Monitoring
Volume 2023, Article ID 9369850, 17 pages
https://doi.org/10.1155/2023/9369850

Research Article

Multispectral Balanced Automatic Fault Diagnosis for Rolling Bearings under Variable Speed Conditions

Wenchang Song,[1] Liang Guo ,[2] Andongzhe Duan,[1] Hongli Gao,[1] Yaoxiang Yu,[1] Tingting Feng,[1] Tao Chen,[1] and Weipeng Ma[1]

[1]*Engineering Research Center of Advanced Driving Energy-Saving Technology, Southwest Jiaotong University, Chengdu 610031, China*
[2]*Engineering Research Center of Advanced Driving Energy-Saving Technology, Ministry of Education, Southwest Jiaotong University, Chengdu 610031, China*

Correspondence should be addressed to Liang Guo; guoliang@swjtu.edu.cn

Received 15 March 2023; Revised 26 June 2023; Accepted 22 September 2023; Published 9 October 2023

Academic Editor: Olivier Bareille

As a key component of machine, most rolling bearings operate under variable speed conditions. Therefore, it is critical to complete automatic fault diagnosis for rolling bearings under variable speed conditions. Although there have been many research studies on fault diagnosis in recent years, the following two problems still exist in fault diagnosis of variable speed bearing: (1) due to the large range of energy distribution for signals under variable speed conditions, the existed signal processing methods lead to the loss of fault information; (2) when directional filtering is carried out according to four different types of faults, the difference in amplitudes of the obtained spectrums is large. This means that the filtering result with the maximum amplitude will be determined as the fault type by mistake. In order to integrate the information scattered across different frequency spectrums and use reasonable filtering to complete automatic diagnosis, Multispectral Balanced Automatic Fault Diagnosis is proposed for rolling bearings under variable speed conditions. On the one hand, signals are preprocessed by the Multispectral Lossless Preprocessing Module, which can eliminate the influence of variable rotating speeds and avoid the loss of fault information. On the other hand, the Balanced Envelope Demodulation Module is designed to realize automatic fault diagnosis by Protrugram and Balancing Envelope Spectrum. The effectiveness of the proposed method is verified by simulated signals and experimental data. Results indicate that the method can complete automatic fault diagnosis of rolling bearings under variable speed conditions with an accuracy of 76%, which outperforms state-of-the-art methods.

1. Introduction

Rolling bearings are widely used in rotating machines, and their dynamic performance plays a significant effect on stability, reliability, and even safety of the machines [1]. Automatic diagnosis of mechanical state based on sensor signals has attracted more and more attention in recent years [2]. Since most rolling bearings work in harsh variable speed conditions, such as motor bearings and axle-box bearings in high-speed trains, it is necessary to carry out bearing fault diagnosis under variable speed conditions [3, 4]. Failure of bearings cause abnormal vibration and noise, which means that vibration signals of rolling bearings carry rich information about their states of health [5]. Therefore, classical fault diagnosis methods evaluated health of equipment through taking time domain or frequency domain indicators of vibration signals under normal conditions as a reference [6, 7]. However, characteristics of signals become more complex under variable speed conditions [8]. Specifically, spectral lines become blurred because of the speed changes; thus, it is difficult to make accurate characteristic frequency analysis to diagnose faults automatically. Consequently, automatic fault diagnosis of rolling bearings under variable speed conditions relies on two conditions: (1) eliminating

the influence of variable speeds; (2) finding an appropriate adaptive filter to complete automatic diagnosis.

In recent years, many researchers proposed methods to eliminate the influence of variable speed conditions. Signal processing methods based on order tracking are widely used. The main step of order tracking is resampling signals at a constant angular increment. Bossley et al. [9] proposed the hardware order tracking (HOT), which resampled equiangular signals of vibration signals by photoelectric encoders and key phasor sensors. Encoder signals could be effectively used for health monitoring of rotating machines [10]. However, the required encoders and key phasor sensors are expensive, and their control circuits are complex. These disadvantages limit its application. Therefore, Kong et al. [11] proposed the calculation order tracking (COT) technology realized by computer. This method is more convenient than the previous one because vibration signals and key phasor signals are collected synchronously by acquisition equipment at equal-time intervals. However, it is difficult to obtain key phasor information in practical applications of this method. Accordingly, Zhao et al. [12] proposed a tacho-less order tracking technique to extract the tachometer information from a low frequency range. Although all methods mentioned above can achieve fault diagnosis under variable speed conditions to a certain degree, they are only applicable for the offline fault detection.

Aiming at this shortcoming, Wang et al. [4] proposed an online tacho-less order tracking method which solved three problems including ridge detection under heavy background noises, online monocomponent extraction, and adaptive bandpass filter. In this method, the instantaneous frequency of harmonics was obtained based on adaptive short-time Fourier transform (ASTFT) and ridge search. Although satisfactory resampling results can be derived when processing simulated signals, ridge line search may fail when processing experimental data. With the development of neural networks, many scholars have chosen deep learning to eliminate the impact of variable speed conditions. Lu et al. [13] proposed a novel fault diagnosis method based on spectrum alignment (SA) and deep transfer convolution neural network (DTCNN), where the SA algorithm that can convert nonstationary vibration signals into stationary signals. After verification, this method has shown good effectiveness and high accuracy in bearing fault diagnosis. However, the premise of this method is that the speed signal is known. In actual operation, the accuracy of the speed information calculated from the impact signals is very poor, which cannot meet the requirements of the SA algorithm.

Furthermore, it is necessary to demodulate signals by filtering to improve signal-to-noise ratio after resampling. Thus, bearing fault diagnosis can be carried out through prominent fault feature frequencies. In recent years, scholars proposed a series of classical demodulation and frequency analysis methods, such as envelope demodulation analysis, spectral kurtosis analysis, wavelet packet demodulation [14, 15], empirical mode decomposition [16, 17], and stochastic resonance theory [18, 19]. The most important problem of filtering is setting parameters of the filter including bandwidth and central frequency. Dwyer [20] proposed frequency domain kurtosis (FDK), which can determine filter parameters to find out fault impulse components in signals. However, the accuracy of this method depended on a reasonable length of analysis segment. Another method calculated the kurtosis of signals in time domain [6]. Among them, the fast kurtosis (FK) showed the best effectiveness [7]. The calculation speed of FK is faster than FDK, and there are fewer hyperparameters as well. However, it is difficult to find out correct filter parameters when the energies of target signals are low and environmental noises are large. Therefore, Barszcz and JabŁoński [21] proposed Protrugram, which was an adaptive method for optimizing filter parameters. In order to extend the conventional diagnosis technique under variable speed conditions, Wang et al. [22] proposed a rotating speed isolation method based on Protrugram. This method took four different fault frequencies of rolling bearings as filter bandwidths and selected the filter center frequency adaptively. However, after Protrugram with different characteristic frequencies, the difference in amplitudes of the obtained spectrums is large. This means that the filtering result with the maximum amplitude will be determined as the fault type by mistake.

At the same time, some scholars have proposed the methods based on deep learning to diagnose the fault of bearings. Compared with traditional methods, intelligent diagnosis can automatically capture useful features from the original signals, instead of manually selecting and extracting them [23]. Lu et al. [24] exploited an explainable one-dimensional convolutional neural network model by combining with the demodulated frequency features of vibration signals and apply it to the fault classification of rolling bearings under time-varying speed conditions. This method divided the input signals into a training set and a testing set. Then, it labeled the training set and trained the intelligent diagnostic model. The accuracy of fault classification obtained by testing the intelligent diagnostic model through a test set is very high. However, the step of labeling the training set must be manually completed. This means that the above deep learning-based methods cannot achieve true automatic diagnosis.

According to the above description, there are two problems about automatic fault diagnosis for rolling bearings under variable speed conditions. On the one hand, the angle-domain resampling method must avoid broken of ridge line search to eliminate the influence of variable speed conditions. On the other hand, amplitudes of signals after filtering need to be unified to make sure that the filtering method can be applied to the automatic diagnosis process. In order to solve these problems, Multispectral Balanced Automatic Fault Diagnosis (MBAFD) is proposed to diagnose faults of rolling bearings under variable speed conditions. The proposed method consists of two modules: Multispectral Lossless Preprocessing Module and Balanced Envelope Demodulation Module.

When speed changes too much, the energy distribution range of signals expand. Intuitively, obvious interruption shows in a single power spectrum, which means that a single power spectrum cannot clearly represent all information in

signals. Consequently, the ridge search of order tracking for a single spectrum fails when speed variation range is too large. However, the original spectrum line is clear when the rotating speed is high, and the envelope spectrum line is clear when the rotating speed is low. In the Multispectral Lossless Preprocessing Module, multispectrum formed by spectrum, envelope spectrum, and known inaccurate speed effectively avoids ridge search failures and then gets resampling signals. Subsequently, the resampling signals are inputted to the Balanced Envelope Demodulation Module. Because four filtered results can be obtained by Protrugram according to four different fault characteristic frequencies, the Balancing Envelope Spectrum (BES) is proposed to eliminate the difference of amplitudes between filtered results. Meanwhile, BES can suppress noises of spectral lines and avoid offset. Therefore, fault types of rolling bearings under variable speed conditions are judged by the Balanced Envelope Demodulation Module. In summary, the fault types of bearings are got by MBAFD after inputting bearing vibration signals.

The rest of this paper is organized as follows. Section 2 introduces the proposed method MBAFD in detail. Section 3 verifies the function of MBAFD with simulation signals and experimental data. Sections 4 and 5 verify the function of MBAFD by open data and self-made test bench data. The conclusions are drawn in Section 6.

2. Multispectral Balanced Automatic Fault Diagnosis

The proposed method consists of two modules: Multispectral Lossless Preprocessing Module and Balanced Envelope Demodulation Module. Multispectral Lossless Preprocessing Module eliminates the influence of variable speed conditions without losing information about the fault. In this module, Multispectral refers to the fusion of spectrum, envelope spectrum, and known inaccurate speed. In the Balanced Envelope Demodulation Module, the Balanced Envelope Spectrum (BES) is constructed to eliminate the difference of amplitudes between filtered results of Protrugram. The framework of the proposed method is shown in Figure 1.

2.1. Multispectral Lossless Preprocessing Module. The energy distribution range of rolling bearing vibration signals is too large under variable speed conditions. Thus, using a single spectrum to analyze bearing fault inevitably leads to fault information loss. Specifically, the original spectrum line is clear when speed is high, and the envelope spectrum line is clear when speed is low in the experiment. Therefore, the information in these two spectrums should be integrated skillfully. In general, it is easy to get inaccurate bearing speed information. Therefore, the inaccurate rotational speed information is used to revise the fitting range in order to avoid descent of precision. The spectral line processing method of multispectrum fusion is proposed to solve this problem in the first module. This module includes the following four steps.

The first step is to use the inaccurate speed information. In this step, the instantaneous frequency and phase are fitted by shock signals as reference information. It is possible to roughly calculate the instantaneous frequency of equipment by counting the number of pulses per second. The smooth speed curve $S[i]$ is obtained by quartic polynomial interpolation. Phase of cumulative rotation is calculated by equation (1).

$$\text{phase}[i] = 2\pi \cdot \sum_{1}^{i} S[i]. \tag{1}$$

If true fundamental frequency or its harmonics are observed near the given imprecise rotational speed, it is possible to extract it and use it as true instantaneous frequency. If not, the difference between estimated instantaneous frequency and rotational speed measured by sensors cannot be too large. To summarize, the multispectrum is formed by fusion of spectrum, envelope spectrum, and known inaccurate speed.

The second step is extracting the target order from the spectrum and envelope spectrum. In order to get envelope spectrum $h(t)$, target signals are Hilbert transformed to obtain their analytical forms firstly: $h(t) = x(t) + iH(t)$. Thereinto, $H(t)$ represents Hilbert transform. Generalized Fourier transform (GFT) is an effective nonstationary signal processing method, which can map the continuously changing components of frequency to a constant target frequency. As a result, general bandpass filtering methods can be used to extract nonstationary components which is easy to mix and difficult to extract [25, 26]. When analyzing signals, it is expected to find out the frequency and amplitude corresponding to the highest energy in every moment. Therefore, original and envelope signals are demodulated based on GFT, and time-domain signals which contained a single component of target order are extracted. For given time-domain signals, the GFT is shown in the following equation:

$$X_G(f) = \int_{-\infty}^{+\infty} x(t) e^{-i2\pi[ft + s_0(t)]} \mathrm{d}t. \tag{2}$$

In equation (2), $s_0(t)$ is a real number function that depends on time. It expresses the evolution process of signals' phase with time. After GFT, the target order of signals is mapped to a component $\tilde{x}_{f_0}(t)$ with certain frequency f_0. Hereinto, f_0 does not change with time. Thus, it is easy to separate it from adjacent orders. Time-domain signals of target order can be obtained by inverse generalized Fourier transform (IGFT) on the extracted $\tilde{x}_{f(0)}(t)$. IGFT is shown in the following equation:

$$\begin{aligned} x(t) &= \int_{-\infty}^{+\infty} X_G(f) e^{i2\pi[ft + s_0(t)]} \mathrm{d}f \\ &= e^{i2\pi s_o(t)} \int_{-\infty}^{+\infty} X_G(f) e^{i2\pi \mathrm{ft}} \mathrm{d}f. \end{aligned} \tag{3}$$

If $X_G(f)$ is equal to $\delta(f - f_0)$, then $s(t)$ is equal to $e^{i2\pi[ft + s_0(t)]}$. It means that signals with the instantaneous frequency of $f(t) = f_0 + s_0'(t)$ and $s_0'(t) = ds_0(t)/dt$ are

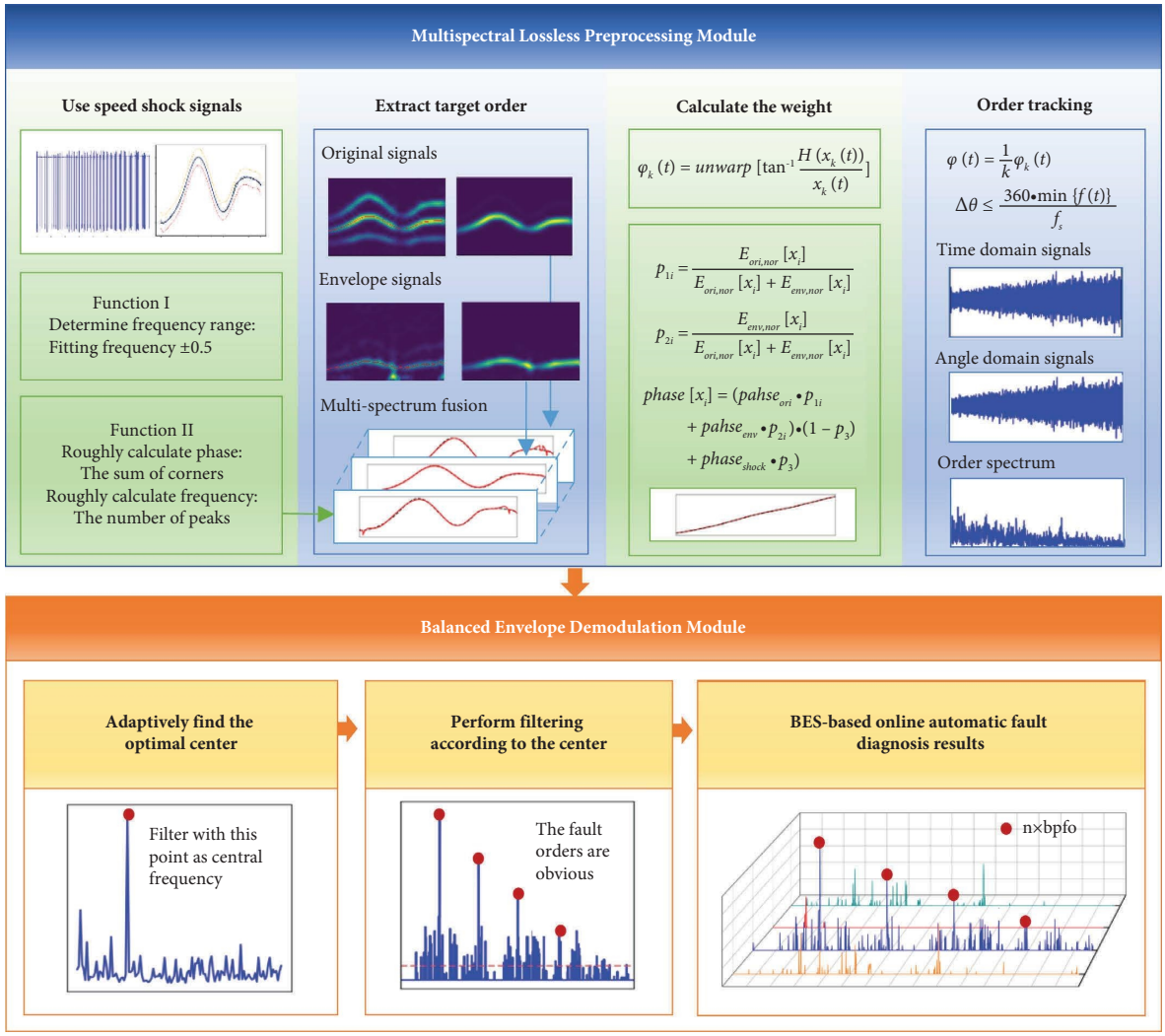

Figure 1: Proposed MBAFD (original figure).

mapped to fixed-frequency signals after GFT. Consequently, it is necessary to find a phase function $s_0(t)$ that satisfies the above conditions. The function is shown in the following equation:

$$s_0(t) = \int_0^T \frac{ds_0(t)}{dt} = \int_0^T f(t) - f_0. \tag{4}$$

The above analysis shows that GFT enables the extraction of harmonic components to be implemented under variable speed conditions. Therefore, original signals and envelope signals are analyzed based on the GFT, and different frequencies are used to fit the corresponding instantaneous phase. What is more, in this step, the instantaneous frequency fitted by velocity shock information is used to determine the range of the ridge search and removed the outliers of the instantaneous frequency fitted by the ridge.

The third step is calculating the instantaneous phase. The target order of time domain obtained in the second step is converted into the angular domain. For single-component time-domain signals $x_k(t)$, the phase is calculated by the following equation:

$$\varphi_k(t) = \text{unwarp}\left[\tan^{-1}\frac{H(x_k(t))}{x_k(t)}\right]. \tag{5}$$

In the formula, unwarp[ ] represents a winding operator, which converts $x_k(t)$ from the $[-\pi, \pi]$ interval to the accumulated phase space. $H(x_k(t))$ represents the Hilbert transform. For the *kth* harmonic of signals, there is a linear proportional relationship between its instantaneous phase $\varphi_k(t)$ and instantaneous phase $\varphi(t)$ of the rotational frequency. Therefore, the instantaneous phase of the rotational frequency is obtained according to the following equation:

$$\varphi(t) = \frac{1}{k}\varphi_k(t). \tag{6}$$

Fitted values of the instantaneous frequencies are obtained by deconvolving time domain signals of the original signals and envelope signals. The power spectrums after IGFT obtained in the second step are normalized to calculate the weight of the two estimated values. Then, the

instantaneous phase obtained by fitting velocity shock signals and two ridge searches are weighted to obtain a more accurate instantaneous phase estimation result. Fitting formulas are shown in the following equation:

$$\begin{cases} \text{phase}[x_i] = (\text{pahse}_{\text{ori}} \cdot p_{1i} + \text{pahse}_{\text{env}} \cdot p_{2i}) \cdot (1 - p_3) + \text{phase}_{\text{shock}} \cdot p_3, \\ p_{1i} = \dfrac{E_{\text{ori,nor}}[x_i]}{E_{\text{ori,nor}}[x_i] + E_{\text{env,nor}}[x_i]}, \\ p_{2i} = \dfrac{E_{\text{env,nor}}[x_i]}{E_{\text{ori,nor}}[x_i] + E_{\text{env,nor}}[x_i]}. \end{cases} \tag{7}$$

Among them, $\text{phase}_{\text{ori}}$, $\text{phase}_{\text{env}}$, and $\text{phase}_{\text{shock}}$ are instantaneous phase information obtained from the original signals, envelope spectrum signals, and speed impact signals, respectively. p is an adaptive confidence. Specifically, p_1 and p_2 are obtained according to the energy-ratio, and p_3 represents the confidence to fit $\text{phase}_{\text{shock}}$ to the final phase estimation result. This paper takes p_3 as 0.3. In addition, $E_{\text{ori,nor}}[x_i]$ and $E_{\text{env,nor}}[x_i]$ are energy values normalized according to maximum values of their respective power spectrums in the calculation process.

The fourth step is resampling and order tracking signals. Instantaneous phases of signals are obtained from the above steps. It establishes correspondence between angle and time. Time position of each equal-angle sampling point can be obtained from its inverse function as shown in equation (8). The deconvolution operation ensures monotonicity of phase change.

$$t_n = \varphi^{-1}(n\Delta\theta). \tag{8}$$

After obtaining coordinates of time points, the signals can be resampled according to the timing position segments. In order to meet requirements of high accuracy and small computation at the same time, the amplitude of each point is not calculated by interpolation during resampling. In addition, the interval of angular domain resampling satisfies the condition shown in equation (9) in order to avoid confusion. Hereinto, f_s is the sampling frequency of original signals and $\min\{f(t)\}$ is the lowest rotation frequency of the axis [21].

$$\Delta\theta \leq \frac{360 \cdot \min\{f(t)\}}{f_s}. \tag{9}$$

In conclusion, Multispectral Lossless Preprocessing Module constructs an adaptive instantaneous phase estimation and order tracking method. Exact instantaneous frequency and instantaneous phase can be analyzed from vibration signals and inaccurate speed information. As a result, signals can be resampled to the angular domain. This module builds a bridge between fixed and variable speed signals in the angular domain. It is a simple and feasible way without wasting accuracy of data.

2.2. Balanced Envelope Demodulation Module. In Section 2.1, the Multispectral Lossless Preprocessing Module is proposed to eliminate the frequency modulation caused by speed changes. Based on the research in Section 2.1, it is necessary to further analyze the resampled signals for fault diagnosis. Therefore, the Balanced Envelope Demodulation Module is constructed to automatically filter resample signals and diagnose fault types.

The most critical step in constructing a filter is to set the center frequency point and bandwidth. The adaptive method for setting filter parameters optimally realized based on Protrugram. Protrugram inherits the advantage of resistance to noise from the spectral kurtosis method. Meanwhile, directional filtering can be completed according to different fault frequencies. The input of the algorithm is spectrum $f(x)$, iteration step s, and bandwidth b_w. Hereinto, $f(x)$ is the spectrum of resampling signals. In order to make the filtered signals contain three harmonics, b_w is equal to 3.5 times the fault characteristic frequency and let $s = 100Hz$. The method looks for location in signals' spectrum where spectral line harmonics are clearest and uses the location as the central frequency point of filter.

It is necessary to calculate the equivalent rotational fundamental frequency f_0 of the axis after resampling for calculating the fault characteristic frequency. In the above section, instantaneous phase $\varphi(t)$ of signals is calculated after resampling. It makes sure that phase function is monotonic. Therefore, the sampling frequency f_s' of new angular domain can be obtained by the following equation:

$$f_s' = \frac{N}{(1/2\pi) \cdot \max(\varphi(t))}, \tag{10}$$

whereinto N indicates the number of sampling points for one actual rotation of axis. The equivalent fundamental frequency f_0 can be calculated by f_s/f_s', and f_s is the original frequency of sampled signals. Four different fault characteristic frequency values can be obtained from the formula of fault characteristic frequency. Then, b_w is obtained, and four directional filtering is performed. After that, four segments' filtered signals are obtained after filtering according to four different fault characteristic frequency

values. As a result, clear characteristic frequencies are extracted and the characteristic frequency spectrum peaks and their harmonic components are observed on its spectrum. However, there is a large difference between amplitudes of four results. When quantitative analyzes spectrum characteristics, it is easy to judge the result with large amplitude as the real fault by mistake. Therefore, in order to comprehensively analyze four results, it is necessary to solve the problem of inconsistent scales.

Aiming at the above problem, this module proposed the Balanced Envelope Spectrum (BES) method to realize automatic fault analysis by the Protrugram optimized spectrum. BES eliminates the difference of scale between different spectrums. It also suppresses noises of the spectral lines and eliminates the offset. The calculation steps of BES are as follows:

(1) Calculating the squared envelope spectrum of the filtered signals by Protrugram.

(2) Scaling amplitudes of spectrums to similar scale intervals. Protrugram performs filtering with a large bandwidth, and the squared envelope spectrum is calculated after filtering to extract the low frequency components well. Therefore, in squared envelope spectrum, the frequency converted part does not include a distinct spectral peak. But it has a certain amount of energy definitely. Scaling by energy, then the creation of equivalent scaling factor parameters can be obtained in different squared envelope spectra of the same signal. Thus, energy peak at observable harmonic is scaled on each squared envelope spectrum.

(3) Subtracting RMS envelope values of the spectrum. This step changes the variance of the spectral lines instead of the characteristics of their Gaussian distribution. It makes the spectral line directly reflect how much each spectral peak is more prominent than other regions. Eventually, the fault threshold is calculated by the 5-sigma method [27].

After the above processing, four-squared envelope spectrums have similar scales. The spectral lines with the highest energy but without an obvious fault characteristic frequency are also suppressed. The spectral lines with smaller energy but the clearest characteristic frequency obtain a larger amplitude scale. Thus, the spectral peaks of characteristic frequency and harmonic are clearly expressed. The spectrum is clean, and the spectrum peak is clear. The effect of BES is as expected which establishes a new balance in the different spectrums after filtering the same signals. The large amplitude makes it easy to recognize outliers [28]. It ensures that the fault type of bearing is clearly judged according to the fault characteristics of each spectrum.

3. Simulation Analysis

In order to verify the performance of the Multispectral Lossless Preprocessing Module under variable speed conditions, simulation signals are constructed by combining the fault mechanism and signal model of rolling bearings, which is shown in Figure 2.

Simulation signals are obtained by the following equation:

$$x(t) = \sum_{i}^{I} A_i S(t-i) + \sum_{n} B_n \cos\left(2\pi n f(t) + \beta_n\right) + \mathrm{wgn}(t). \tag{11}$$

$\sum_i^I A_i S(t-i)$ indicates the sequence of shocks caused by failure. A_i is the amplitude of the ith shock, and signals of fault shock in the measured time period include the superposition of the first i shocks. It is assumed that the outer ring of a rolling bearing is fixed, the inner ring rotates with a shaft, and the failure occurs in the outer ring of the bearing. Bearings generate exponentially decaying shock signals when passing fault position, as shown in (12). Simulated shock signals are shown as Figure 2(a). The second part of (12) represents the fundamental frequency and harmonics of the system. Failure characteristic frequency is set at 3 times of rotational frequency, and the angular interval between each shock is 120°. Superposition signals of shock signals and harmonic signals and signals with noise are shown as Figures 2(b) and 2(c). Instantaneous frequency and confidence range is in Figure 2(d).

$$s(t) = e^{-\alpha t} \sin\left(2\pi f_r t\right). \tag{12}$$

The power spectrum is obtained by short-time Fourier transform and square operation of simulated signals. Energy information can be used as fault characterization [29]. The basic, second, and third harmonics are clearly identified in Figure 3(a). The energy of the second harmonic is the largest obviously. The results of GFT on the second harmonic are shown in Figure 3(b), where second harmonic signals are mapped to constant frequency signals. After bandpass filtering of constant frequency signals, the second harmonic is obtained and interference of the first and third harmonics is excluded. The results are shown in Figure 3(c). Then, IGFT is performed on filtered signals, and results of power spectrum are shown in Figure 3(d).

The information of envelope signals is shown in Figure 4, where (a) shows original signals, (b) shows signals after the Hilbert transform, and (c) is the envelope spectrum of original signals. For envelope signals obtained by the above transformation, results of the ridge search on power spectrum are shown in Figure 5(a). It is clear that signal characteristics in the low frequency band are enhanced. Therefore, the second harmonic frequency is fitted by ridge search results of enveloped signals. Remaining processing steps are all similar to the steps of original signals' processing. Because envelope signals are mapped to constant frequency signals by GFT, signals of doubled frequency are obtained by filter and IGFT, and results are shown in Figures 5(b)–5(d).

The next step is calculating confidence coefficients of original and envelope signals. The two power spectrums of original and envelope signals are normalized according to their maximum values. Consequently, the confidence coefficients are obtained according to energy share.

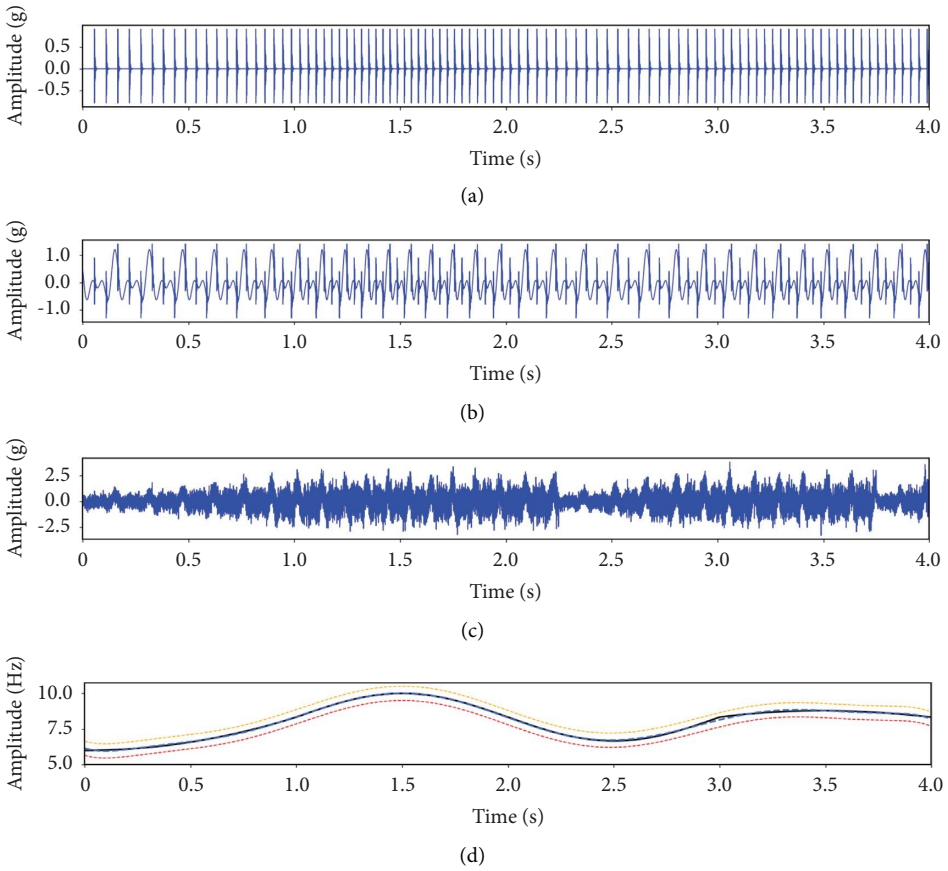

Figure 2: Simulation signal: (a) simulated shock signals; (b) superposition of simulated shock signals and harmonic signals; (c) superposition of simulated shock signals, harmonic signals, and noise; (d) instantaneous frequency and confidence range.

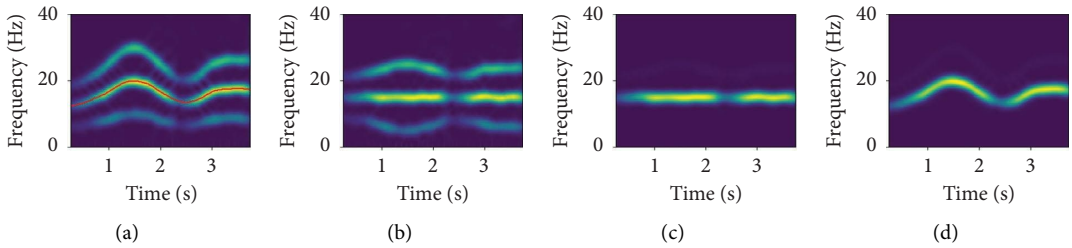

Figure 3: Power spectrum of simulation signal: (a) original signal and its ridge search; (b) GFT; (c) filtering; (d) IGFT.

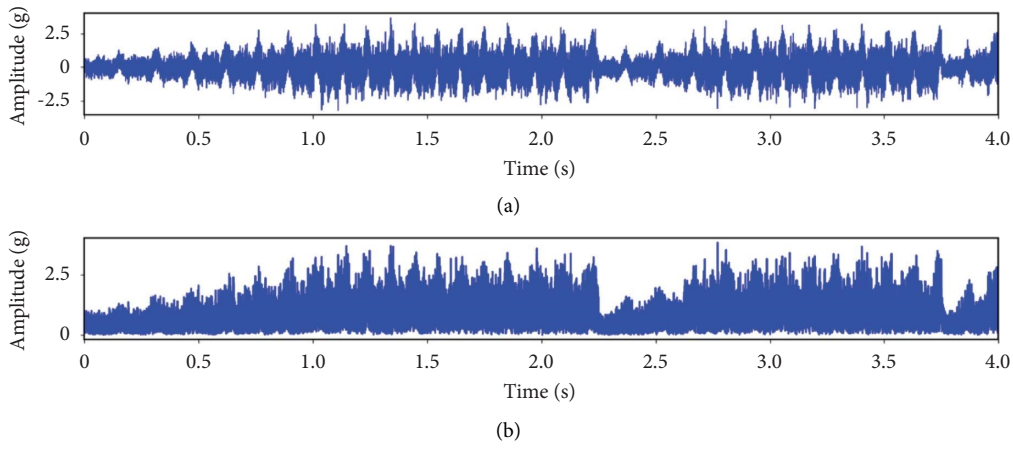

Figure 4: Continued.

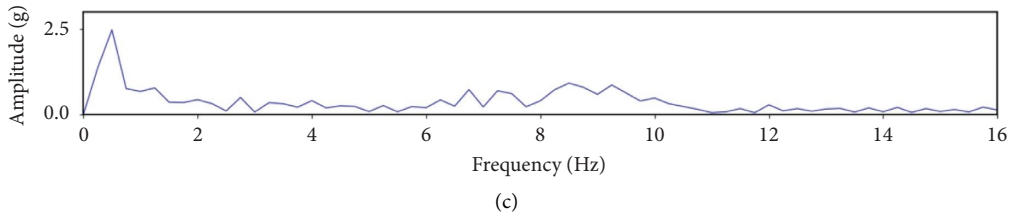

Figure 4: (a) Original signals; (b) envelope signals; (c) envelope spectrum.

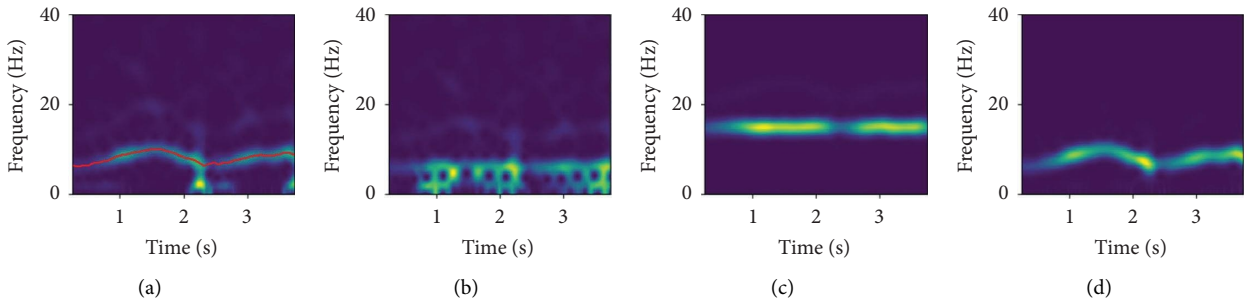

Figure 5: Power spectrum of envelope spectrum: (a) envelope signals and ridge; (b) GFT; (c) filtering; (d) IGFT.

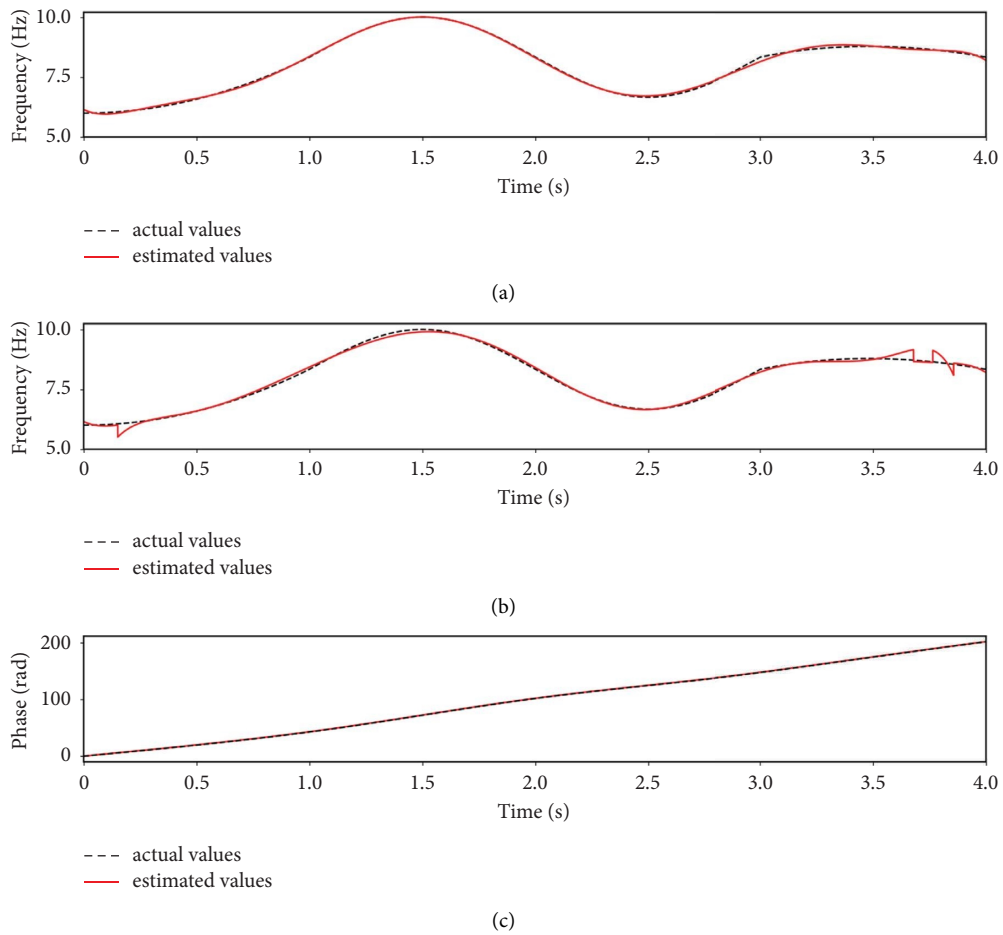

Figure 6: Comparison between actual values and estimated values: (a) frequency estimated from the original signals; (b) frequency estimated from the envelope spectrum; (c) fitted instantaneous phase values.

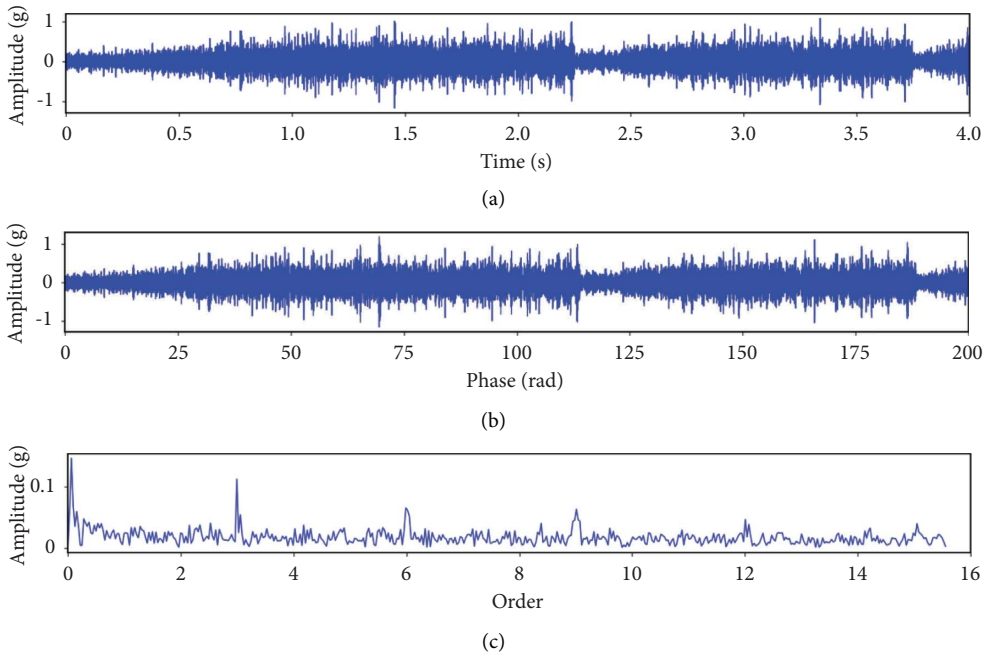

Figure 7: The results of the multispectral lossless preprocessing module: (a) the signals before resampling; (b) the results of resampling; (c) order spectrum.

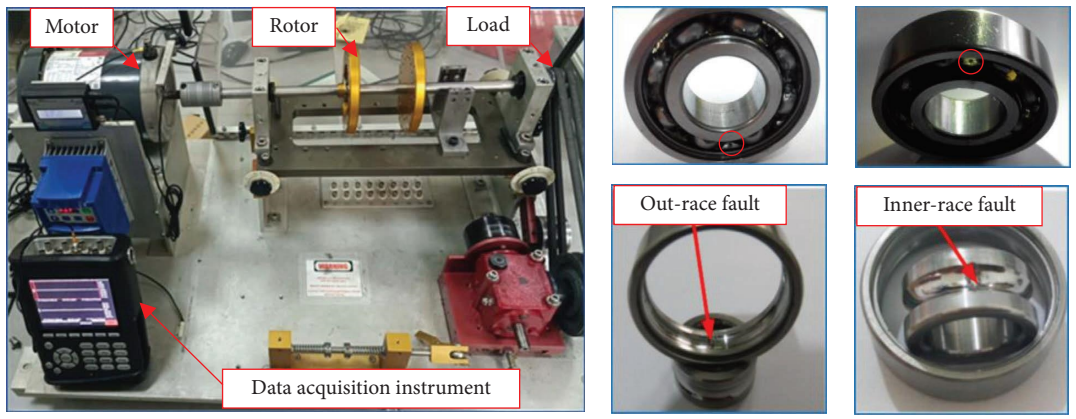

Figure 8: Test bench for the variable speed spectra quest [30].

Instantaneous phase signals are fitted according to the confidence degree. The comparison between the fitted result and the real instantaneous frequency is shown in Figure 6. Obviously, this method accomplishes more accurate order tracking. The fitted instantaneous phase signals are resampled into the angular domain at an interval of 10 radians. Resampling results are shown in Figures 7(a) and 7(b). After resampling of signals, the order tracking results can be obtained as shown in Figure 7(c). The fourth order of outer ring failure is seen clearly in Figure 7(c). Therefore, it proves that the accurate instantaneous frequency and phase can be obtained by combining original signals and envelope signal spectrums.

4. Experiment Case 1: SQV Dataset

In this section, the SQV variable-speed bearings dataset of Xi'an Jiaotong University [30] is analyzed to verify performance of MBAFD. As is shown in Figure 8(a), the test bench based on laboratory simulation for variable-speed spectra quest (VSQ) is composed of a servomotor, rotors, an acceleration sensor, a CoCo80 data-gathering device, and load imposed by a tensioned belt. A total of six types of faults are simulated, including the inner race fault (IF) and outer race fault (OF) under three different damage degrees, respectively. Photos of faulty bearings are shown as Figures 8(b) and 8(c). A group of outer race fault data (REC3495) is used to verify the feasibility of MBAFD. In

Table 1: Details of experiment case 1.

Data number	Fault type	Area (mm^2)	Depth (mm)
REC3477	Outer race fault	12	2
REC3478	Outer race fault	12	2
REC3479	Outer race fault	12	2
REC3495	Outer race fault	8	1
REC3533	Inner race fault	12	2
REC3534	Inner race fault	12	2
REC3535	Inner race fault	12	2

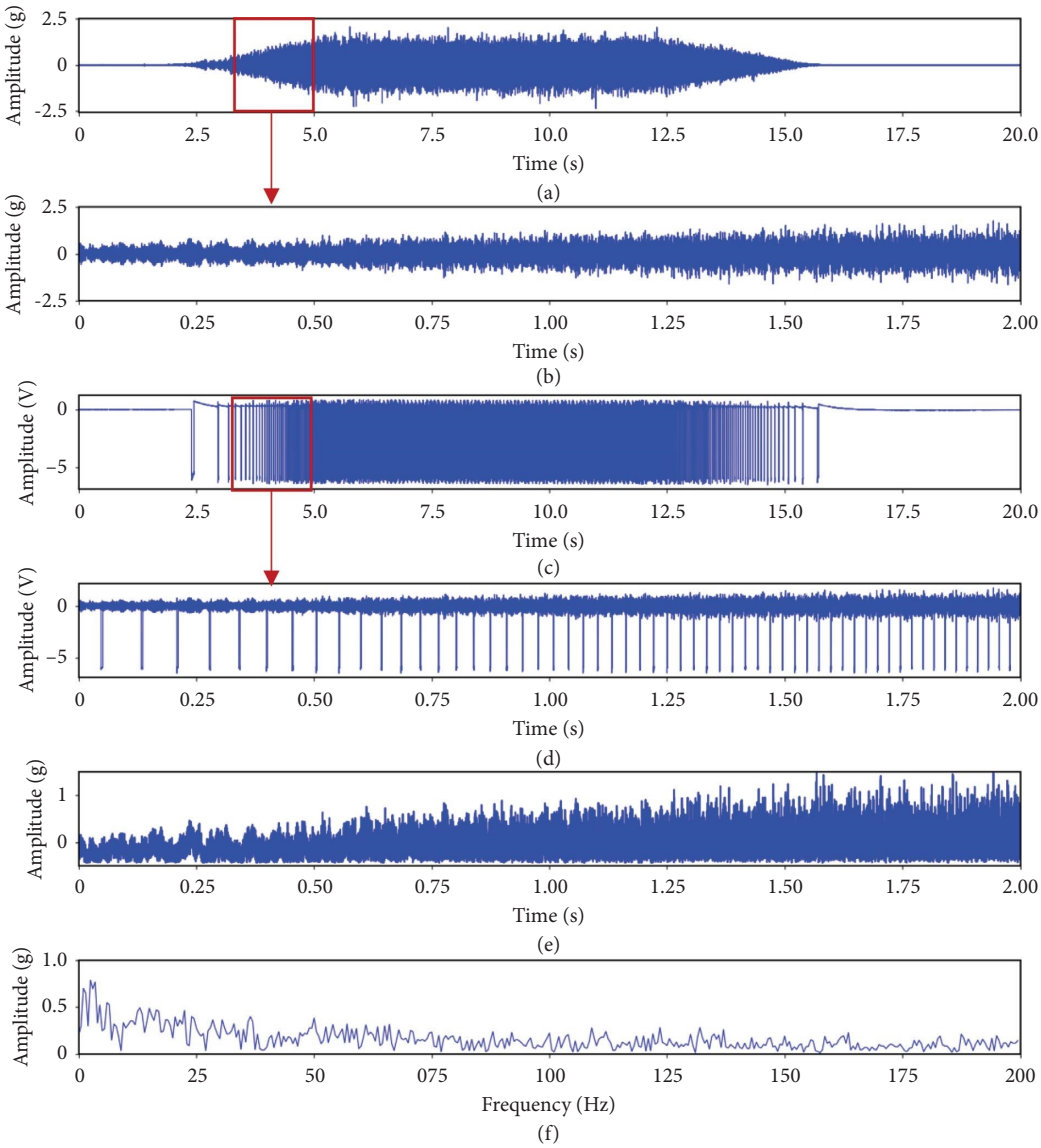

Figure 9: Signals of test variable-speed bearings data: (a) vibration signals; (b) vibration signals segment; (c) shock signals; (d) shock signals segment; (e) envelope signals; (f) envelope spectrum.

addition, three groups of inner race bearing fault (REC3533-REC3535) and three groups of outer race bearing fault (REC3477-REC3479) are used to verify the accuracy of MBAFD. As shown in Table 1, the bearings used in this section have different fault types and sizes.

The experimental data include vibration signals and impact signals corresponding to bearing failure. The bearing model is SNK6203. Figures 9(a) and 9(c) show vibration signals and shock signals of a 20-second segment, and Figures 9(b) and 9(d) show a selected 2-second segment. Hereinto, (e) shows signals after Hilbert transform, and (f) is the envelope spectrum of 2-second signals.

Figures 10(a) and 10(c) show the power spectrum of intercepted and envelope signals. Figures 10(b) and 10(d)

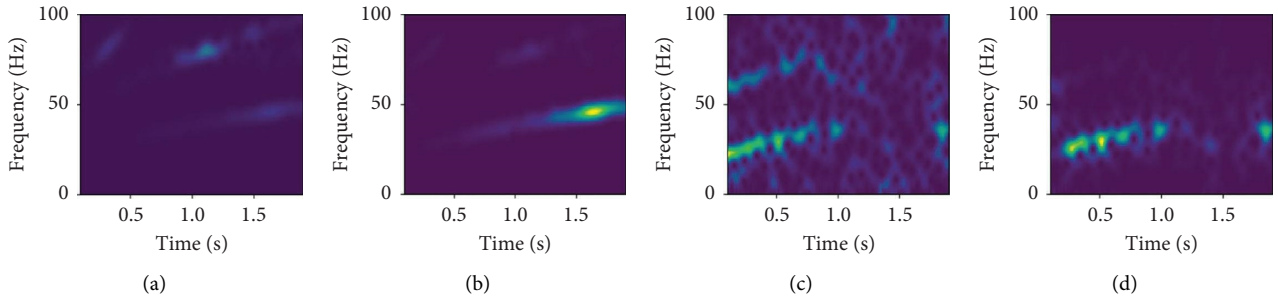

Figure 10: Power spectrum: (a) original signals before GFT and IGFT; (b) signals after GFT and IGFT; (c) envelop signals before GFT and IGFT; (d) envelop signals after GFT and IGFT.

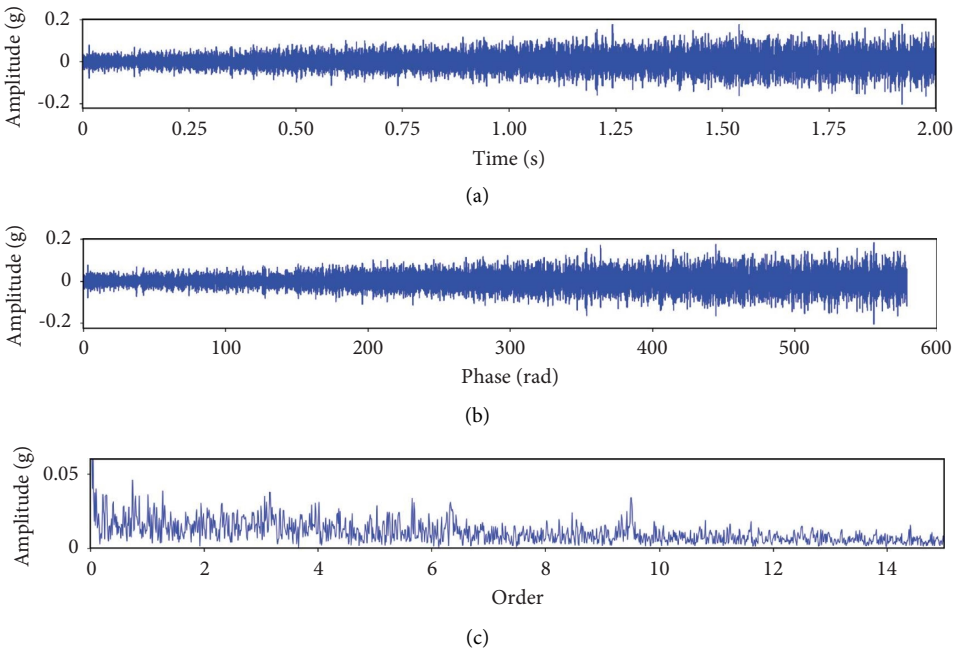

Figure 11: Results of the multispectral lossless preprocessing module: (a) original signals; (b) the results of resampling; (c) order spectrum after resampling.

show the results of GFT, filtering, and IGFT. Results show that instantaneous power spectrums of original signals clearly reflect the information with higher energy in the second half of the time series. Power spectrum of envelope signals can clearly characterize the information with lower energy in the first half. The above analysis shows that the approach to combine original and envelope signals is meaningful in analyses. The results of resampling and order tracking are shown in Figure 11, where (a) shows original signals, (b) is the result of resampling, and (c) is the result of order tracking. Time domain signals under variable speed conditions are transformed into angular domain smooth signals. Meanwhile, the order of signals becomes obvious.

Figure 12(a) shows Protrugram plots after order tracking optimized by BPFI, BSF, FTF, and BPFO equivalent characteristic frequency and corresponding bandwidth. Figure 12(b) shows the envelope spectrums of signals after filtering according to the optimal center frequency point calculated by Protrugram. As shown in the figure, the envelope spectrum obtained by analyzing BPFO as the characteristic frequency shows the clearest characteristic frequency spectrum peak. The Protrugram aimed at BPFI, which has a similar center frequency point and a wider bandwidth to the BPFO filter, also shows the fault characteristic frequency to some extent.

Figure 12(c) shows the envelope spectrums after BES, and the red line means RMS development of each spectrum. In the BES spectrum filtered by BPFO, the fault characteristic frequencies are well observed and the rest of spectrums do not reach the condition to determine any fault. Then, fault threshold used to determine the spectral peak is calculated by the 5-sigma method. The red line in Figure 12(d) shows the determination thresholds at 5 times the standard deviation, above which the BES spectrum has a significant peak. To reduce the probability of misclassification of normal sample as fault, the sample is determined as a fault sample only when the characteristic frequencies all exceed the threshold. Figure 12(e) synthetically shows the balanced envelope spectrum. The

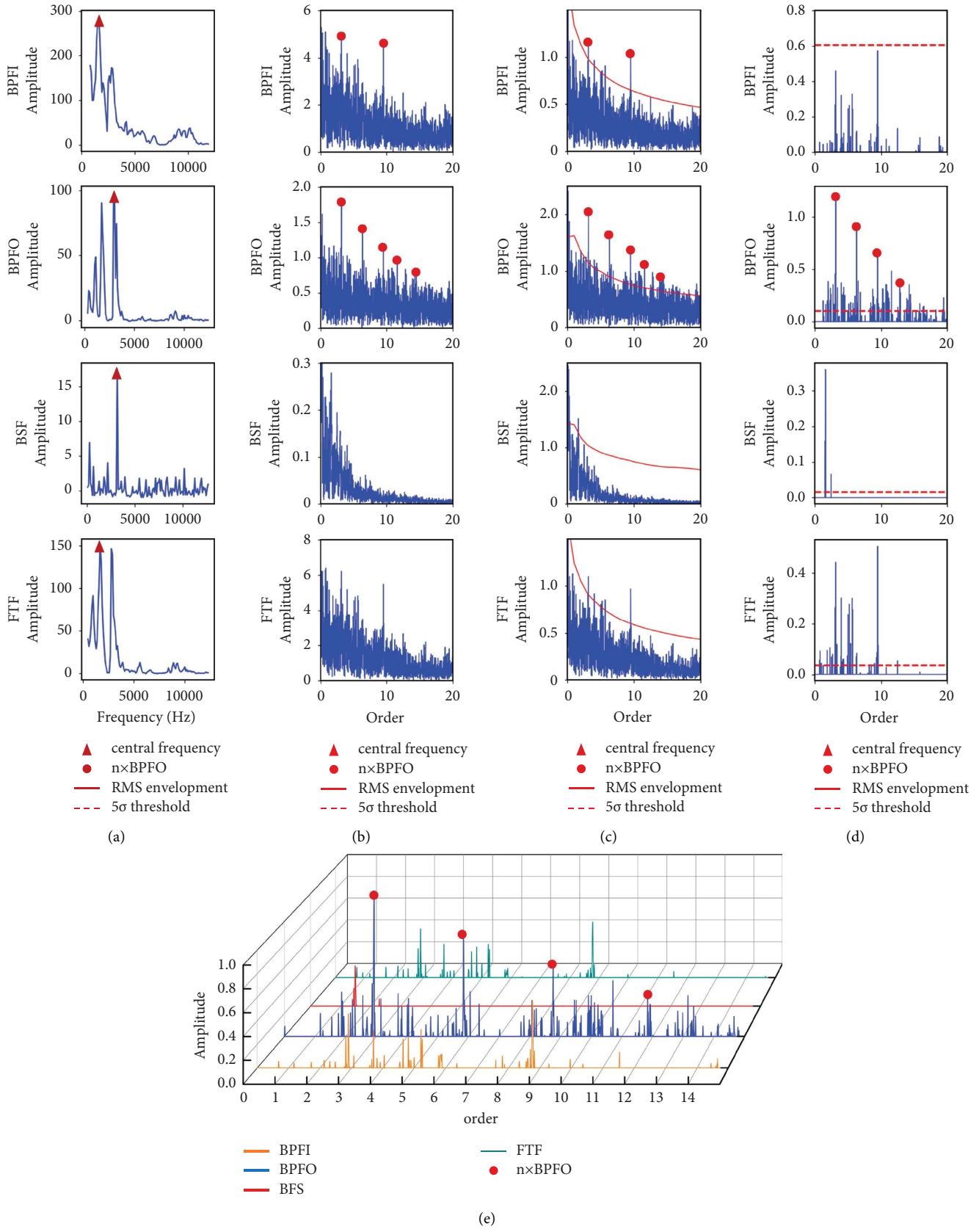

FIGURE 12: Filtering process and results: (a) Protrugram kurtosis spectrum and optimal center frequency; (b) Protrugram; (c) each characteristic frequency is scaled according to the frequency conversion energy; (d) threshold and fault determination; (e) balanced envelope spectrum.

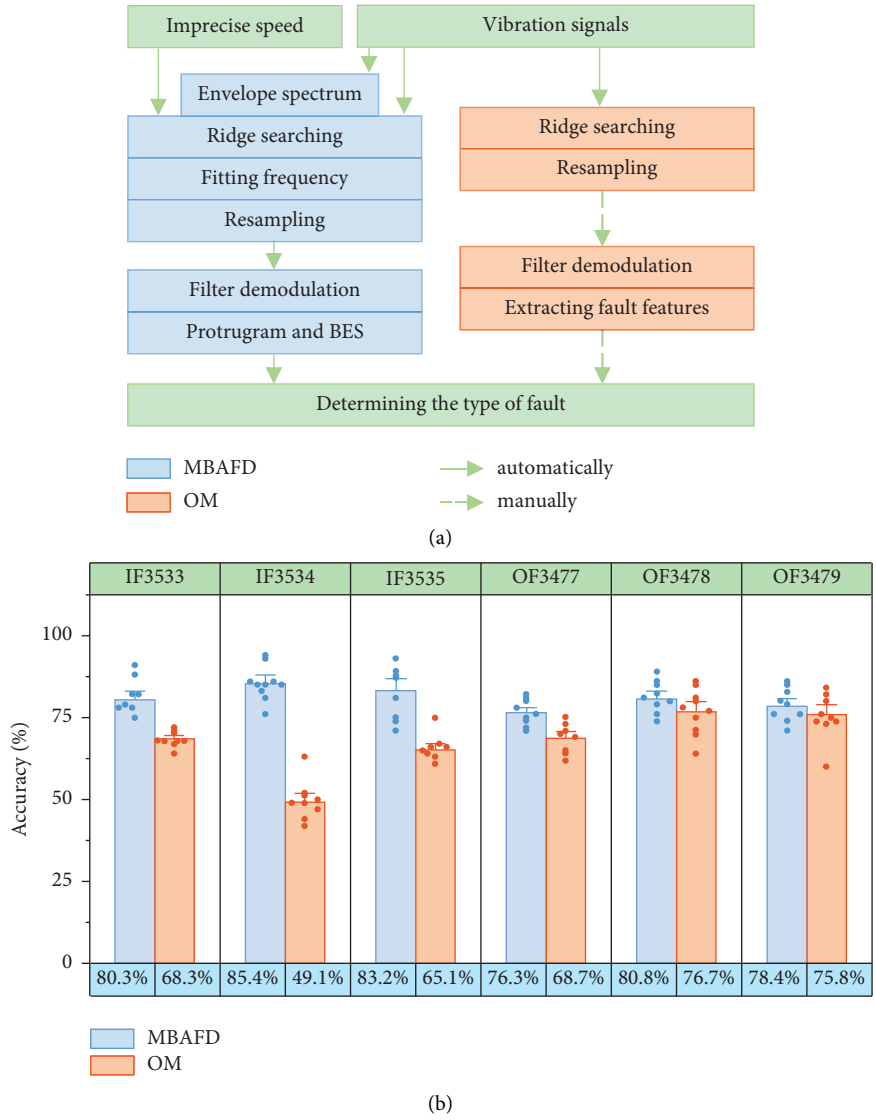

FIGURE 13: Comparison of MBAFD and original method (OM) by the SQV dataset: (a) the process of two methods; (b) diagnostic accuracies of two methods.

following phenomena can be seen from the figure: (1) envelope spectrums have a similar scale; (2) offset of the original FTF spectral line with high bottom noise and low energy is removed; (3) the BSF spectral line with high energy but no obvious fault characteristics is suppressed; (4) the BPFO spectral line with less energy but the clearest Eigen frequency achieves the largest amplitude. In conclusion, spectral lines are generally clean and spectral peaks are clear.

In addition, three groups of inner race bearing fault data (REC3532-REC3537) and three groups of outer race bearing fault data (REC3477-REC3479) are used to verify the accuracy rate of the proposed method in inner and outer ring fault diagnosis. Ten segments are selected randomly during speed variation of each data set. The proposed method and the original method are applied to conduct 100 experiments on each segment, respectively. The comparison of process and diagnostic accuracy between the proposed method (MBAFD) and the original method (OM) [31] is shown in Figure 13.

It can be seen from Figure 13(a) that the original method has the following shortcomings. On the one hand, only the vibration signals are used for ridge search. On the other hand, the filtering parameters need to be set manually and the amplitudes of signals after filtering are not unified. However, the proposed MBAFD fits more signals to avoid information loss and ridge search failure, simultaneously using Protrugram and BES to complete automatic directional filtering and unified amplitudes. The above steps can be automatically completed with a given bearing size. The points in Figure 13(b) represent diagnostic accuracies of corresponding signals' segment. The histograms represent the average accuracy of ten signal segments. As shown in the figure, fault diagnosis accuracy of the proposed method is much higher than that of the original method in every group. When the proposed method is applied to inner ring fault diagnosis, the average accuracy rate is 82.9%, which is 22.1% higher than the original method. When the proposed method is applied to

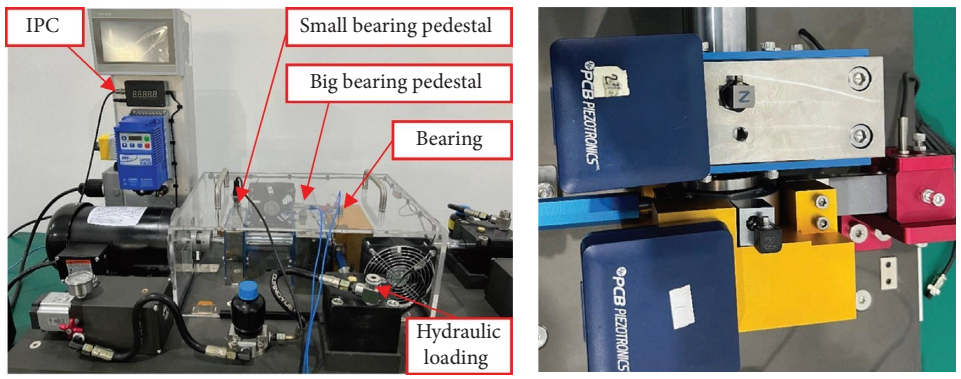

(a) (b)

Figure 14: (a) Test bench for bearing life-cycle signals' acquisition; (b) sensor installation diagram (original photographs).

Table 2: Details of experiment case 2.

Data number	Fault type	Radial load (kg)	Rotational frequency (Hz)
3301000	Rolling element fault	1000	30
4350600	Rolling element fault	600	35
6351000	Rolling element fault	1000	35

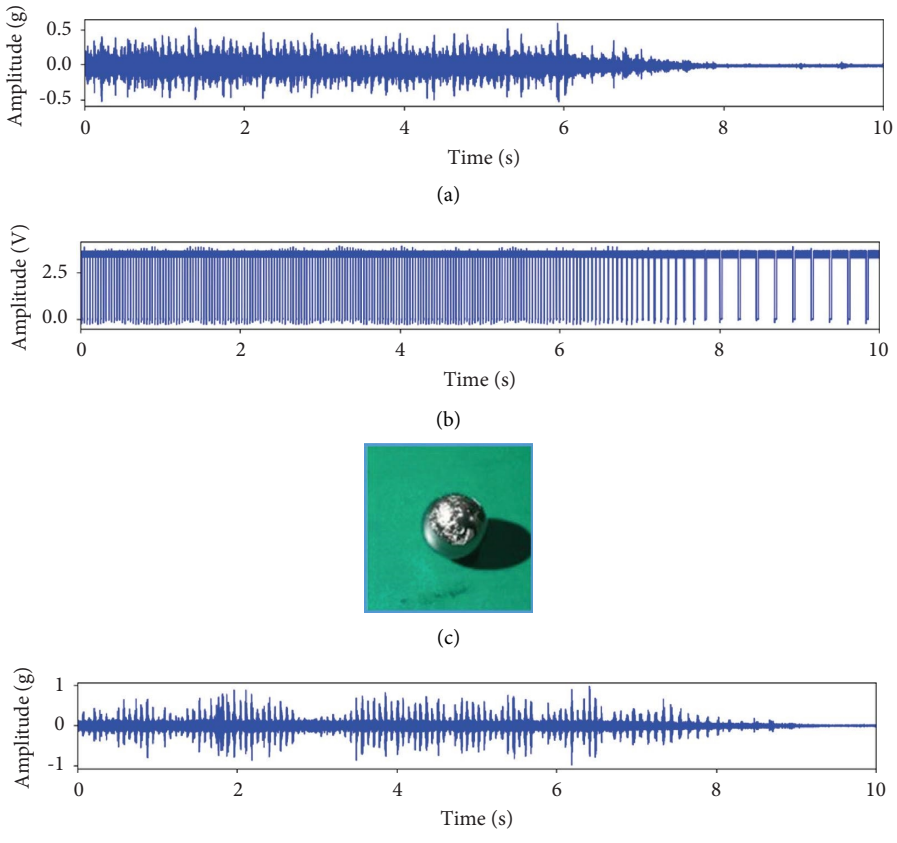

Figure 15: Continued.

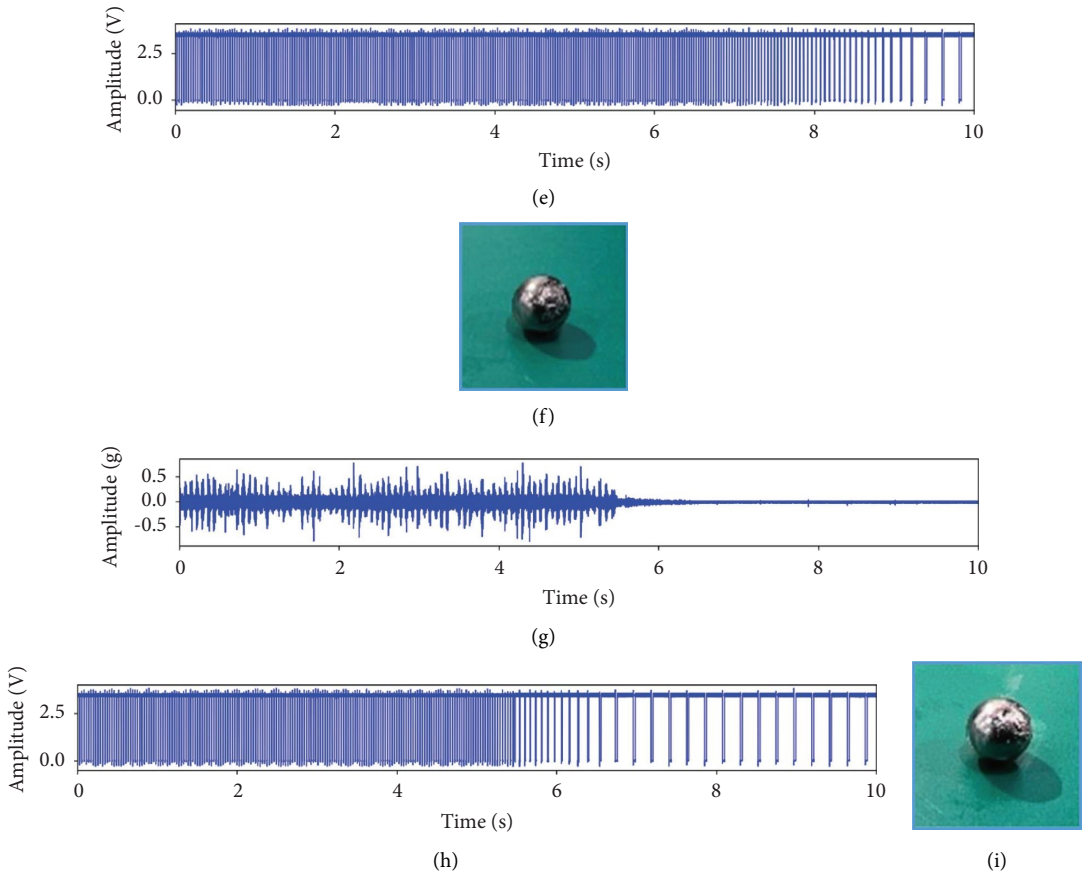

Figure 15: Signals and faults of three bearings: (a), (d), and (g) vibration signals; (b), (e), and (h) shock signals; (c), (f), and (i) failure photos (original photographs).

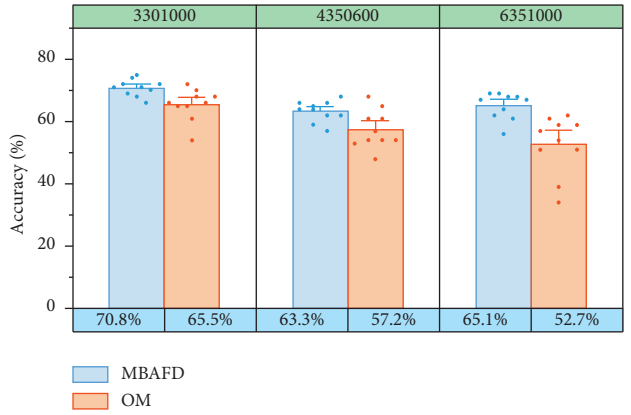

Figure 16: Comparison of diagnostic accuracy of MBAFD and original method (OM) about bearing experiment.

outer ring fault diagnosis, the average accuracy rate is 78.5%, which is 4.8% higher than the original method.

5. Experiment Case 2: Bearing Experiment

In order to further verify the accuracy of MBAFD diagnosis, a test bench is built as shown in Figure 14(a). The bearing model used in the experiment is ER-16K. The accelerometer PCB 356A15 is installed to collect vibration signals in z direction of the small bearing pedestal and x, y, z directions of test bearings and large bearing pedestal. Photoelectric sensor is used to collect bearing speed pulse signals. Sensor installation diagram is shown in Figure 14(b). Eight channel signals were collected in this set of experiments, and the final file had 9 columns of data.

The sampling frequency is 25600 Hz. Six bearings were tested until they fail, and three bearings with only rolling element failure are selected for analysis. The details of the experiment are summarized in Table 2.

The obtained life-cycle signals of the three failed bearings with rolling element failure. Vibration signals are shown in Figures 15(a), 15(d), and 15(g). Shock signals are shown as Figures 15(b), 15(e), and 15(h). Photographs of the corresponding faults are shown in Figures 15(c), 15(f), and 15(i). Select 5-second deceleration segments, respectively, to verify diagnostic accuracy of the proposed and original method. The verification method is randomly selecting ten 2-second segments from 5-second segments to repeat the experiment. We repeat the experiment for 100 times for every 2-second segment and calculate the accuracy of the MBAFD and original method.

The experimental results are shown in Figure 16. Hereinto, points represent fault diagnosis accuracy of different methods for each 2-second signal segment and histograms represent the mean of accuracy rates. As shown in the figure, fault diagnosis accuracy of the proposed method is much higher than the original method in every group. When the proposed method is used for rolling element failure diagnosis under variable speed conditions, the average accuracy rate is 66.4%, which is 7.9% higher than the original method.

6. Conclusion

This paper proposed a new method MBAFD to diagnose fault of rolling bearings automatically under variable speed conditions. The method consists of two modules. On the one hand, the Multispectral Lossless Preprocessing Module is designed to eliminate the influence of variable speed conditions and avoid the loss of information. On the other hand, the Balanced Envelope Demodulation Module is designed to realize automatic fault diagnosis by Protrugram and Balancing Envelope Spectrum (BES). Experiment of simulated signals, SQV dataset, and bearing experiment were used to verify the efficiency and accuracy of the proposed method. Several conclusions can be drawn from the above results.

(1) Multispectral Lossless Preprocessing Module can resample vibration signals of rolling bearings under variable speed conditions without the loss of fault information. This module obtains the instantaneous phase based on the original spectrum, envelope spectrum, and velocity information and then implements resampling and order tracking.

(2) Balanced Envelope Demodulation Module is designed to diagnose faults of bearings automatically. In this module, the Protrugram-based algorithm can select the optimal filtering center frequency point automatically and BES can unify amplitudes of filtered spectrums. The results show that this method is able to extract a clear characteristic frequency to diagnose the type of fault automatically.

(3) Compared with neural network-based automatic fault diagnosis methods and traditional signal processing methods, the proposed method has better scientific and engineering value. From a scientific perspective, the generalization and interpretability of the proposed method are better than neural network-based methods. From an engineering perspective, neural network-based methods require a large amount of data to train the model, and the lack of actual fault data limits their application. The proposed method only needs to know the size of the bearing in advance to diagnose the type of fault automatically. Meanwhile, the proposed MBAFD has higher accuracy than traditional signal processing methods.

In conclusion, the proposed MBAFD with the Multispectral Lossless Preprocessing Module and Balanced Envelope Demodulation Module integrates information scattered in different frequency spectrums and uses reasonable filter to complete automatic diagnosis of rolling bearings under variable speed conditions.

Data Availability

The SQV data used to support the findings of this study are available from the corresponding author upon request. The bearing experiment data used to support the findings of this study have not been made available because the project is under security stage.

Conflicts of Interest

The authors declare that they have no conflicts of interest.

Acknowledgments

This research was supported by the National Natural Science Foundation of China (52275134).

References

[1] D. F. Shi, L. S. Qu, and N. N. Gindy, "General interpolated fast fourier transform: a new tool for diagnosing large rotating machinery," *Journal of Vibration and Acoustics*, vol. 127, no. 4, pp. 351–361, 2005.

[2] L. Guo, Y. Yu, M. Qian, R. Zhang, H. Gao, and Z. Cheng, "FedRUL: a new federated learning method for edge-cloud collaboration based remaining useful life prediction of machines," *IEEE*, vol. 28, no. 1, pp. 350–359, 2023.

[3] Y. Liu, Z. Chen, J. Ning, K. Wang, and W. Zhai, "Improved dynamics model of locomotive traction motor with elasticity of rotor shaft and supporting bearings," *Chinese Journal of Mechanical Engineering*, vol. 35, no. 1, pp. 90–359, 2022.

[4] Y. Wang, G. Xu, A. Luo, L. Liang, and K. Jiang, "An online tacholess order tracking technique based on generalized demodulation for rolling bearing fault detection," *Journal of Sound and Vibration*, vol. 367, pp. 233–249, 2016.

[5] Y. Wang and M. Liang, "An adaptive SK technique and its application for fault detection of rolling element bearings," *Mechanical Systems and Signal Processing*, vol. 25, no. 5, pp. 1750–1764, 2011.

[6] J. Antoni and R. B. Randall, "The spectral kurtosis: application to the vibratory surveillance and diagnostics of rotating machines," *Mechanical Systems and Signal Processing*, vol. 20, no. 2, pp. 308–331, 2006.

[7] J. Antoni, "Fast computation of the kurtogram for the detection of transient faults," *Mechanical Systems and Signal Processing*, vol. 21, no. 1, pp. 108–124, 2007.

[8] J. Lin and L. Qu, "Feature extraction based on morlet wavelet and its application for mechanical fault diagnosis," *Journal of Sound and Vibration*, vol. 234, no. 1, pp. 135–148, 2000.

[9] K. Bossley, R. Mckendrick, C. Harris, and C. Mercer, "Hybrid computed order tracking," *Mechanical Systems and Signal Processing*, vol. 13, no. 4, pp. 627–641, 1999.

[10] M. Zhao, X. Jia, J. Lin, Y. Lei, and J. Lee, "Instantaneous speed jitter detection via encoder signal and its application for the diagnosis of planetary gearbox," *Mechanical Systems and Signal Processing*, vol. 98, pp. 16–31, 2018.

[11] Q. Kong, K. Song, and Y. Chen, "Engine speed change stage vibration signal time-frequency analysis of order tracking study," *Journal of Vibration Engineering*, vol. 18, no. 4, pp. 448–452, 2005.

[12] M. Zhao, J. Lin, X. Wang, Y. Lei, and J. Cao, "A tacho-less order tracking technique for large speed variations," *Mechanical Systems and Signal Processing*, vol. 40, no. 1, pp. 76–90, 2013.

[13] F. Lu, Q. Tong, Z. Feng, and Q. Wan, "Unbalanced bearing Fault Diagnosis under various speeds based on spectrum alignment and deep transfer convolution neural network," *IEEE Transactions on Industrial Informatics*, vol. 19, no. 7, pp. 8295–8306, 2023.

[14] H. Qiu, J. Lee, J. Lin, and G. Yu, "Wavelet filter-based weak signature detection method and its application on rolling element bearing prognostics," *Journal of Sound and Vibration*, vol. 289, no. 4-5, pp. 1066–1090, 2006.

[15] W. Su, F. Wang, H. Zhu, Z. Zhang, and Z. Guo, "Rolling element bearing faults diagnosis based on optimal Morlet wavelet filter and autocorrelation enhancement," *Mechanical Systems and Signal Processing*, vol. 24, no. 5, pp. 1458–1472, 2010.

[16] D. Yu, J. Cheng, and Y. Yang, "Application of EMD method and Hilbert spectrum to the fault diagnosis of roller bearings," *Mechanical Systems and Signal Processing*, vol. 19, no. 2, pp. 259–270, 2005.

[17] Y. Lei, Z. He, and Y. Zi, "EEMD method and WNN for fault diagnosis of locomotive roller bearings," *Expert Systems with Applications*, vol. 38, no. 6, pp. 7334–7341, 2011.

[18] Q. He, J. Wang, Y. Liu, D. Dai, and F. Kong, "Multiscale noise tuning of stochastic resonance for enhanced fault diagnosis in rotating machines," *Mechanical Systems and Signal Processing*, vol. 28, pp. 443–457, 2012.

[19] Q. He and J. Wang, "Effects of multiscale noise tuning on stochastic resonance for weak signal detection," *Digital Signal Processing*, vol. 22, no. 4, pp. 614–621, 2012.

[20] R. F. Dwyer, "A technique for improving detection and estimation of signals contaminated by under ice noise," *Journal of the Acoustical Society of America*, vol. 74, no. 1, pp. 124–130, 1983.

[21] T. Barszcz and A. JabŁoński, "A novel method for the optimal band selection for vibration signal demodulation and comparison with the Kurtogram," *Mechanical Systems and Signal Processing*, vol. 25, no. 1, pp. 431–451, 2011.

[22] Y. Wang, G. Xu, Q. Zhang, D. Liu, and K. Jiang, "Rotating speed isolation and its application to rolling element bearing fault diagnosis under large speed variation conditions," *Journal of Sound and Vibration*, vol. 348, pp. 381–396, 2015.

[23] Y. Yu, L. Guo, Y. Tan, H. Gao, and J. Zhang, "Multisource partial transfer network for machinery fault diagnostics," *IEEE Transactions on Industrial Electronics*, vol. 69, no. 10, pp. 10585–10594, 2022.

[24] F. Lu, Q. Tong, Z. Feng et al., "Explainable 1DCNN with demodulated frequency features method for fault diagnosis of rolling bearing under time-varying speed conditions," *Measurement Science and Technology*, vol. 33, no. 9, Article ID 095022, 2022.

[25] X. Xiong, S. Yang, and C. Gan, "A new procedure for extracting fault feature of multi-frequency signal from rotating machinery," *Mechanical Systems and Signal Processing*, vol. 32, pp. 306–319, 2012.

[26] Z. Chen, L. Guo, H. Gao et al., "A fault pulse extraction and feature enhancement method for bearing fault diagnosis," *Measurement*, vol. 182, 2021.

[27] N. Li, Y. Lei, J. Lin, and S. X. Ding, "An improved exponential model for predicting remaining useful life of rolling element bearings," *IEEE Transactions on Industrial Electronics*, vol. 62, no. 12, pp. 7762–7773, 2015.

[28] L. Guo, Y. Huang, H. Gao, and L. Zhang, "Ball screw fault detection and location based on outlier and instantaneous rotational frequency estimation," *Shock and Vibration*, vol. 2019, Article ID 7497363, 12 pages, 2019.

[29] B. Muruganatham, M. Sanjith, B. Krishnakumar, and S. Satya Murty, "Roller element bearing fault diagnosis using singular spectrum analysis," *Mechanical Systems and Signal Processing*, vol. 35, no. 1-2, pp. 150–166, 2013.

[30] S. Liu, J. Chen, S. He, Z. Shi, and Z. Zhou, "Subspace Network with Shared Representation learning for intelligent fault diagnosis of machine under speed transient conditions with few samples," *ISA Transactions*, vol. 128, pp. 531–544, 2022.

[31] H. Chen, Y. Zhang, and B. Huang, "A bearing fault diagnosis method based on order tracking under variable speed operating conditions," *The Test and Application*, vol. 12, pp. 49–55, 2021.